# Near-Threshold Electron Attachment as Regge Resonances: Cross Sections for K, Rb, and Cs Atoms†

**Alfred Z. Msezane,*,‡ Zineb Felfli,‡ and Dmitri Sokolovski§**

*Department of Physics and Center for Theoretical Studies of Physical Systems, Clark Atlanta University, Atlanta, Georgia 30314, School of Mathematics and Physics, Queen's University of Belfast, Belfast, BT7 1NN, UK*

*Received: July 11, 2007; In Final Form: September 24, 2007*

We investigate the near-threshold formation of negative ions as Regge resonances in electron−atom scattering, with specific results obtained for $e^-$−K, $e^-$−Rb, and $e^-$−Cs. The complex angular momentum method, implemented within the Mulholland formulation of the total elastic cross sections, is employed. We demonstrate that for $e^-$−K, $e^-$−Rb, and $e^-$−Cs scattering, the near-threshold electron attachment cross sections are characterized by the Wigner threshold behavior, Ramsauer−Townsend minima, and Regge resonances, all discernible only through Regge partial cross section scrutiny. Regge partial, differential, and total elastic cross sections are presented and contrasted, as well as the differential cross section critical minima.

## I. Introduction

Cold collisions, those with collision energies below ~1 $cm^{-1}$ [1 meV = 8.0655 $cm^{-1}$ = 96.485 J $mol^{-1}$], provide deep insight into quantum dynamics and imply the dominance of only a very few partial waves in the collision.[1] Cold electron collisions, resulting in negative ion formation, occur naturally in terrestrial and stellar atmospheres as well as in industrially important plasmas for device fabrication. Reliable atomic and molecular affinities are also necessary for the understanding of a vast number of chemical reactions involving negative ions.[2] Collisional phenomena, such as elastic and inelastic scattering, reactive collisions, spin polarization, and rotational and vibrational state changes, can occur in the cold regime, manifesting pronounced quantum-mechanical effects.[3] A variety of interesting physical effects associated with low temperatures include elastic collision rates and chemical reactions at vanishing temperatures.[4]

The importance of the $\ell = 2$ resonance in cross sections for spin-flipping transition and elastic scattering in the low-energy collisions involving structureless atoms and molecules has been determined,[5] including the possibility of the direct effect of the spin-flipping transitions on the buffer-gas loading of ultracold molecules. These predictions are expected to impact significantly the choice of molecules for experiments at cold and ultracold temperatures.[6] There, molecules may be transparent to electrons, such as when 90 meV electrons go through $CF_4$ unimpeded, demonstrating the importance of the Ramsauer−Townsend (R−T) effect.[1] Rapid sympathetic cooling has been accomplished in a microtrap,[7] leading to the measurement of the $^{40}K-^{87}Rb$ cross sections and the observation of its R−T reduction. In addition, natural fermions present new opportunities for producing ultracold molecules, such as RbCs and investigating fundamental forces.[6] Recently, electron-induced chemistry (dissociative electron attachment) has been explored in phenyl azide,[8] with other fragments, such as $N_3^-$ and $CN^-$ being observed at higher energies and interpreted as proceeding via low-lying shape resonances or higher core-excited resonances.

Thus, the understanding and delineation of atomic and molecular resonance structures at low electron impact energies are important and needed in electron collisions and ion−atom and atom−molecule collisions, etc., including the identification of the R−T minima to guide the creation of molecules and the determination of elastic collision rates and chemical reactions.

This paper explores in the near-threshold energy region the Wigner threshold law,[9] the Ramsauer−Townsend minima, resonances, and the dominant orbital to which the electron preferentially attaches itself to form the temporary negative ions ($K^-$, $Rb^-$, or $Cs^-$) as Regge resonances[10,11] in $e^-$−K, $e^-$−Rb, and $e^-$−Cs scattering. The critical minima of the differential cross sections (DCSs), defined as the values where the differential cross sections have their smallest values as functions of the impact energy, $E$, and scattering angle, $\theta$, are also investigated. Here, we probe electron attachment at its fundamental level using Regge trajectories[12] calculated within the complex angular momentum (CAM) representation of scattering.

Attachment of a very weakly bound electron by the polarization potential of the neutral state[13] produces intershell-type resonances. In particular, K has an enormous dipole polarizability, causing the appearance of an extra characteristic minimum in its generalized oscillator strength;[14] consequently, other peculiarities could be anticipated. Recently, it has been demonstrated through the low-energy electron scattering by $N_2O$ that sufficient representation of polarization effects can yield the measured shape resonance and a Ramsauer−Townsend minimum.[15] The Wigner threshold law[9] is essential in high-precision measurements of binding energies of valence electrons using photodetachment threshold spectroscopy,[16] and recently, the s-wave Wigner law has been observed, accompanied by a d-wave component.[17] The critical minima in electron elastic scattering have also attracted experimental attention.[18]

Regge pole analysis has been applied to atom−atom,[19] electron−atom,[20] and reactive atom−diatom[21] scattering through the Mulholland formula[22] to understand the low-energy oscillations in the total elastic cross section (TCS). Recently, it has

† Part of the "William A. Lester, Jr., Festschrift".
‡ Clark Atlanta University.
§ Queen's University of Belfast.

10.1021/jp075416e CCC: $40.75 
Published on Web 11/30/2007

been used for a fundamental understanding of the near-threshold electron attachment mechanism in $e^-$−Fr and $e^-$−Cs,[23] capturing easily and unambiguously the main results of the Dirac R-matrix[24] and predicting new manifestations. Very recently, sinusoidal Regge oscillations have been demonstrated in short-lived resonances in the $F + H_2$ reaction.[25]

## II. Theory

Following Sokolovski et al.,[20] we consider the presence of a sufficiently narrow resonance, which allows the collision partners to form a long-lived intermediate complex that rotates as it decays at zero scattering angle to preserve the total angular momentum. For the resonance to contribute a peak to the total cross section, two resonance conditions must be satisfied: (i) Regge trajectory[12] (namely, the imaginary part versus the real part of the complex angular momentum) stays close to the real axis and (ii) the real part of the Regge pole is close to an integer. For a system trapped in a resonance state formed by the collision partners, the total scattering cross section (atomic units are used throughout and our energies are measured relative to the ground state of the atom),

$$\sigma_{\text{tot}} = 2\pi k^{-2} \sum_{L=0}^{\infty} (L + 1/2)|1 - S(E)|^2 \qquad (1)$$

is, through the optical theorem,

$$\sigma_{\text{tot}} = 4\pi k^{-1}\, \text{Im}(f(0)) \qquad (2)$$

where $S(E)$ and $f(0)$ are, respectively, the S-matrix and the scattering amplitude.

For our investigation, we use the Mulholland formula[22] implemented within the complex angular momentum representation of scattering in the form[19,20]

$$\sigma_{\text{tot}}(E) = 4\pi k^{-2} \int_0^{\infty} \text{Re}[1 - S(\lambda)]\lambda \, d\lambda - 8\pi^2 k^{-2} \sum_n \text{Im} \frac{\lambda_n \text{Res}_n S}{1 + \exp(-2\pi i \lambda_n)} + I(E) \qquad (3)$$

where $S$ is the S-matrix; $k = (2mE)^{1/2}$, with $m$ being the mass; and $I(E)$ contains the contributions from the integrals along the imaginary $\lambda$-axis and is given in Sokolovski et al.[20] If the lifetime of the complex that is proportional to $1/\text{Im}(L)$, is sufficiently long for the complex to return to the forward direction many times, then Im $\lambda_n \ll 1$ must be satisfied, and for constructive addition,

$$\text{Re}\lambda_n \approx 1/2,\ 3/2,\ 5/2,\ ....$$

or

$$\text{Re}L \cong 0,\ 1,\ 2,\ ...$$

Thus, a resonance is likely to affect the total elastic cross section when its Regge pole position is close to a real integer.

For our investigation, we use the Thomas−Fermi (TF) potential in the form[26]

$$U(r) = \frac{-Z}{r(1 + aZ^{1/3}r)(1 + bZ^{2/3}r^2)} \qquad (4)$$

where $Z$ is the nuclear charge, and $a$ and $b$ are adjustable parameters. For small $r$, the potential describes the Coulomb attraction between an electron and a nucleus, $U(r) \sim -Z/r$, whereas at large distances, it mimics the polarization potential, $U(r) \sim -1/(abr^4)$. For the numerical computation, we have selected the parameters $a = 0.2$, $b = 0.04$. The effective potential, with $\ell = \text{Re}L$ is given by

$$V(r) = U(r) + \ell(\ell + 1)/r^2 \qquad (5)$$

For $\ell = 0$, $V(r)$ is a potential well whose asymptotic behavior supports a finite number of bound states.[20] The numerical results were obtained using the method of Burke and Tate.[27] The robustness of the TF potential with respect to the variation of the parameters $a$ and $b$ has been investigated for e−Ar and e−Kr elastic scattering,[20] and the results compared very well with those of Savukov.[28] It was concluded that eq 4 captures the essential physics (Ramsauer−Townsend minima, the Wigner threshold law, and resonances) when used with the appropriate parameters.

Clearly, to contribute to the forward scattering amplitude, the wave must return to the forward direction a sufficient number of times, and

$$\text{Im}\, L \ll 1.$$

This should provide a signature of the resonance in $\sigma_{\text{tot}}(E)$. It must be noted, however, that Im $L$ cannot be too small, since if it tends to zero, the resonance becomes a bound state, which is by assumption inaccessible to the incident particle under the present consideration. Consequently, Im $L$ should not be significantly small for a meaningful analysis of the collision; otherwise, the residue in eq 3 would correspondingly vanish in this limit.

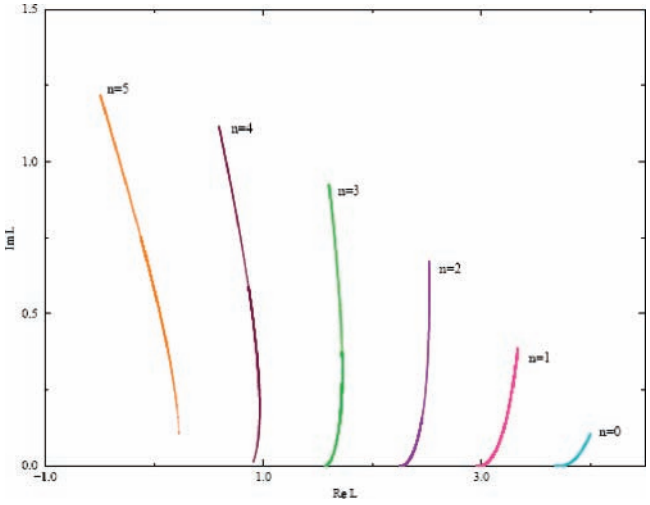


**Figure 1.** Regge trajectories, Im $L(E)$ versus Re $L(E)$ for $K^-$.

## III. Results

For clarity and easier interpretation of the various results, we have decided to present the data for each system separately. Glancing through the various relevant figures, the appropriate comparisons can readily be made and conclusions drawn.

**$e^-$−K.** For the near-threshold electron−K attachment process, the six Regge trajectories, calculated using the method of Burke and Tate,[27] originating from the bound states supported by the Thomas−Fermi potential are shown in Figure 1. Figure 1 shows that only the $n = 5$, $n = 4$, $n = 1$, and $n = 0$ trajectories pass near integer values Re $L = 0$, Re $L = 1$, Re $L = 3$, and Re $L = 4$, respectively. Consequently, they should contribute to the elastic TCS. The $n = 5$ trajectory with Re $L \approx 0$ and Im $L \approx 0.23$ does so at an energy $E \approx 0.056$ eV and is partly responsible

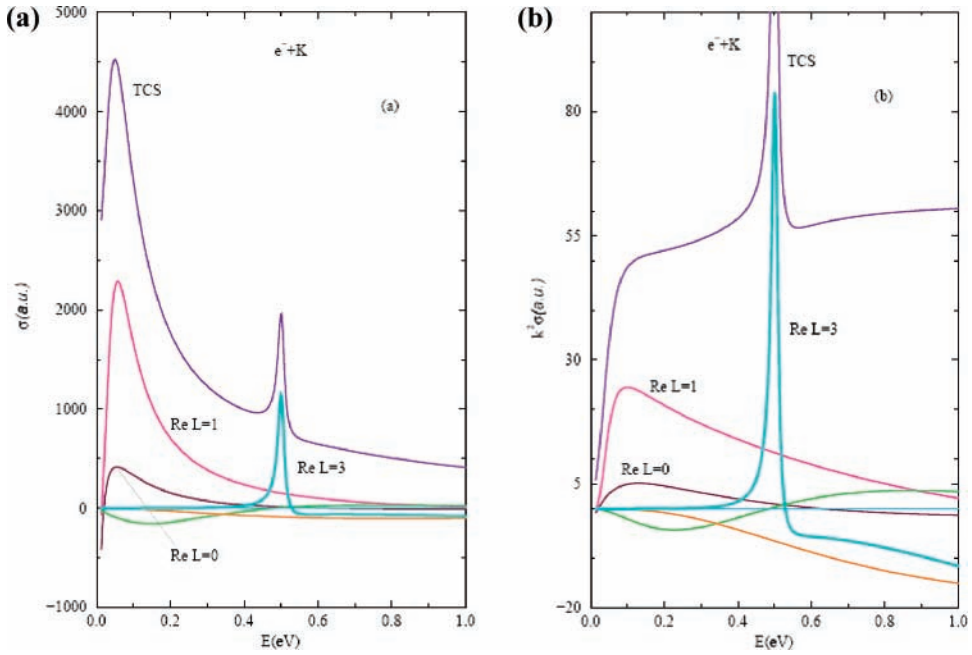


**Figure 2.** (a) The total and partial elastic cross sections, in atomic units, for $e^-$−K versus $E$(eV), showing the Mulholland contributions. (b) The total and partial elastic cross sections, in atomic units, for $e^-$−K, multiplied by $k^2$ (eV) versus $E$(eV), showing the Mulholland contributions.

for the first resonance in the TCS at $E \approx 0.050$ eV in Figure 2a. The $n = 4$ trajectory goes near Re $L = 1$ and Im $L = 0.072$ at an energy of $E \approx 0.058$ eV and is the main contributor to the shape resonance $E \approx 0.050$ eV. The $n = 1$ trajectory, with Re $L = 3$ and Im $L = 0.0009$, accounts for the long-lived resonance at $E \approx 0.50$ eV (note the smallness of the Im L here, implying a longer angular life), while the $n = 0$, Re $L = 4$, and Im $L = 0.05$ gives rise to the resonance at $E \approx 4.99$ eV and falls outside the energy range of Figure 2a. The remaining two trajectories, which do not go near approximate integer values, are expected to have insignificant contributions to the elastic TCS, which is shown in Figure 2a. Also shown in the figure are the Mulholland contributions (individual terms in eq 3) associated with the Regge trajectories.

For a better understanding of the dynamics of the near-threshold electron attachment and to provide a plausible interpretation of the structure in the total elastic cross section behavior, we first multiply the Regge partial cross sections and the TCS by $k^2$ and plot the results, as shown in Figure 2b, covering the energy range $0 \leq E \leq 1.0$ eV. This also enables us to explore the Wigner threshold behavior for $K^-$. We note that in Figure 2a, the shape resonance in the TCS at $E \approx 0.05$ eV is followed by a minimum at $E \approx 0.43$ eV, a long-lived resonance at $E \approx 0.50$ eV, and finally, a broad maximum at $E \approx 4.99$ eV (not shown).

At very low energies, a difficult region to access experimentally, the dominant contribution to the TCS comes from an s-wave (Re $L = 0$), as expected, also clearly demonstrating and firming the Wigner threshold behavior. However, at about $E = 0.62$ eV, the s-wave Regge partial cross section goes to zero, creating the R−T minimum. But the f-wave cross section in this energy region of the R−T minimum affects significantly the position, magnitude, and shape of the Ramsauer−Townsend minimum, as exhibited by the results of Figure 2a. Clearly, the near-threshold dynamic interplay among the s-, p-, and f-wave Regge partial cross sections modifies the position, magnitude, and shape of the R−T minimum. In addition, the plots in Figure 2b demonstrate unequivocally the s-wave Wigner threshold law; the absence of the Regge partial cross sections scrutiny could lead to an incorrect conclusion; namely, that of multiple Wigner threshold behavior for the TCS if only the TCS is considered. In this very low energy region, the active electron attaches itself preferentially to s, p, and f orbitals centered at $E \approx 0.056$, $\approx 0.058$, and $\approx 0.50$ eV, respectively.

In Figure 3, we present the 3-D DCS in both angle and energy, emphasizing the highly peaked phase and showing the structure near threshold. Interestingly, a careful examination of the DCS near threshold does lead to the determination of the critical minima.[10] Figure 4 clearly demonstrates the position of the DCS's critical minimum, found at $E \approx 0.50$ eV and $\theta = 180°$. In addition, for all the angles shown in Figure 4 ($\theta = 0°$, 90°, and 180°) the resonance corresponding to Re $L = 3$ is clearly visible in the DCSs at $E \approx 0.50$ eV, being most prominent at $\theta = 180°$.

**$e^-$−Rb.** Here, we have reinvestigated the robustness of the $e^-$−Rb scattering with respect to the variation of the polarization potential and have used the values $a = 0.2$ and $b = 0.041$; the details are found in Sokolovski et al.[20] Briefly, the eight Regge trajectories, Im $L$ versus Re $L$, originating from the bound states supported by the potential in eq 5 are presented in Figure 5, with the farthest one corresponding to the ground state of $U(r)$. The present results are represented as dashed curves, whereas those of Felfli et al.[29] are denoted as solid curves where differences exist. The figure demonstrates that only the $n = 0$, 1, and 4 trajectories pass near integer values of Re $L = 5$, 4, and 2, respectively. The $n = 4$ trajectory does so at the energy $E = 0.435$ eV and is responsible for the first dominant resonance in the TCS near threshold. The $n = 1$ trajectory with Re $L = 4$ accounts for the sharp resonance at $E = 1.727$ eV, and the $n = 3$ trajectory is responsible for the broad resonance centered at about $E = 7.3$ eV. We note that although the $n = 3$ trajectory is not so close to the Re $L = 3$ value, like the others considered above, it nevertheless has a significant residue component to contribute the broad resonance at approximately $E = 7.3$ eV (not shown in Figure 6a), not visible in the TCS but quite so in the Regge partial cross section.

As has already been indicated,[29] the $n = 0$ trajectory also gives rise to a resonance, but its position is at too high an energy for consideration here; therefore, it is not shown in Figure 6a. The remaining four trajectories do not approach integer values

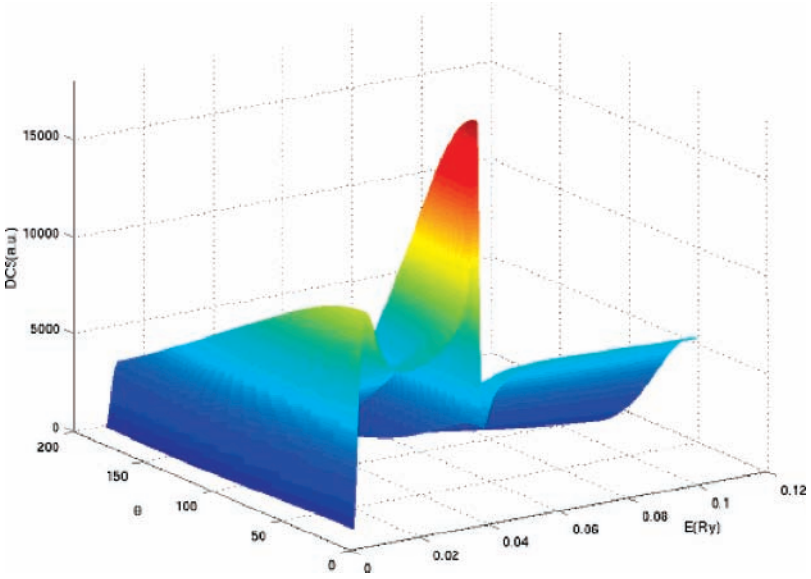


**Figure 3.** Three−D differential cross sections for elastic e⁻−K scattering versus $E$(Ry) and $\theta$(degrees).

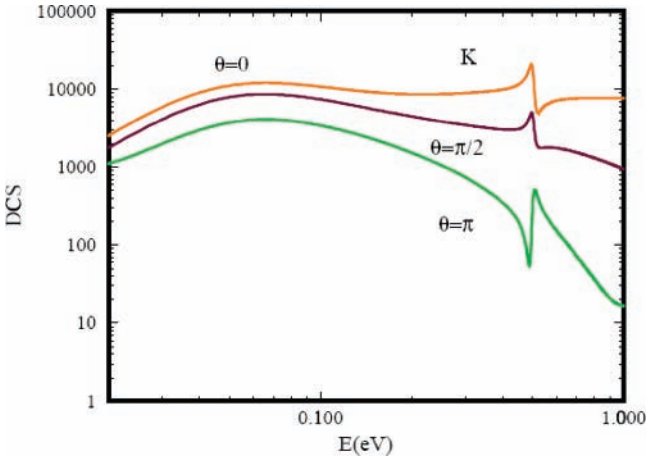


**Figure 4.** Differential cross sections for elastic e⁻−K scattering versus $E$(eV) at $\theta = 0°$, 90°, and 180° showing the DCS's critical minimum.

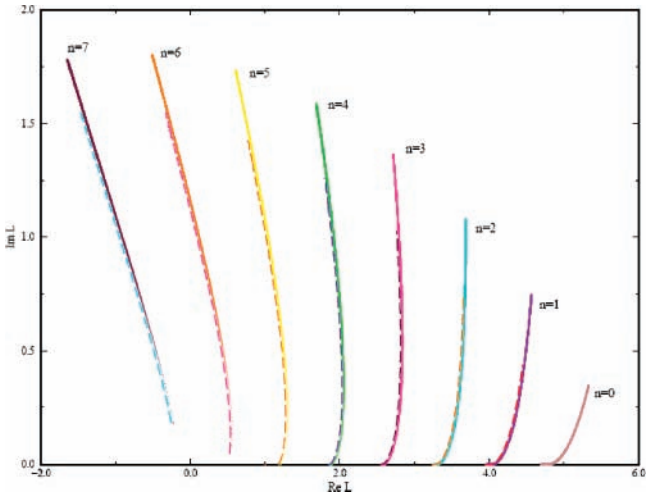


**Figure 5.** Regge trajectories, Im $L(E)$ versus Re $L(E)$ for $Rb^-$ (dashed curves represent present results, and continuous curves are those of ref 21).

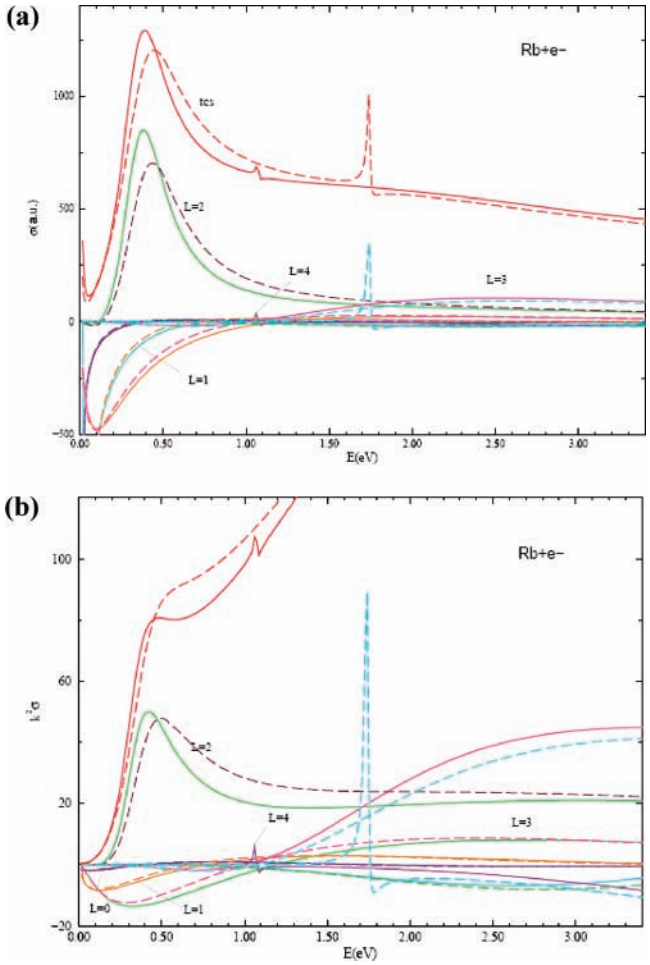


**Figure 6.** (a) The total and partial elastic cross sections, in atomic units, for e⁻−Rb versus $E$(eV), showing the Mulholland contributions (dashed curves represent present results, and continuous curves are those of ref 21). (b) The total and partial elastic cross sections, in atomic units, for e⁻−Rb, multiplied by $k^2$ (a.u.) versus $E$(eV), showing the Mulholland contributions (dashed curves represent present results, and continuous curves are those of ref 21).

and are expected to have much smaller effects on the total elastic cross section. The Mulholland contributions, associated with the Regge trajectories (individual terms in the sum of eq 3), are also plotted in Figure 6a together with the TCS and are compared with the recent results.[29] Clearly, the $n = 4$, 1, and 3 trajectories are responsible for the peaks at $E = 0.435$, 1.727, and 7.3 eV (values not shown), respectively.

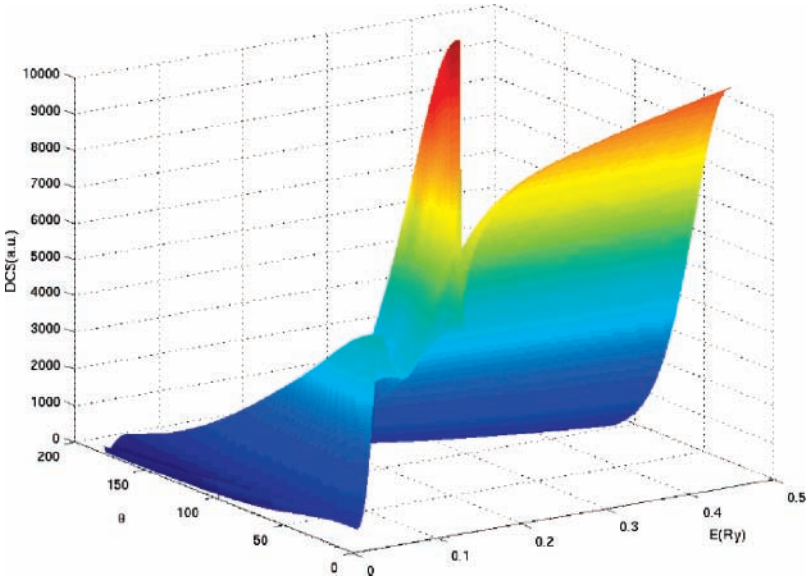


**Figure 7.** Three−D differential cross sections for elastic e⁻−Rb scattering versus $E$(Ry) and $\theta$ (degrees).

From Figure 6a, it is clear that the $n = 4$ trajectory is responsible for the resonance near threshold as well as the Ramsauer−Townsend minimum, both detectable through the TCS. Indeed, the incident electron attaches itself predominantly to a d orbital near threshold, which also defines the resonance and the Ramsauer−Townsend minimum. Our calculated position of the Ramsauer−Townsend minimum of 0.0408 eV is in agreement with that of the Dirac R-matrix value of 0.041 eV[24] and in reasonable accord with the 0.0476 eV obtained by Felfli et al.[29] The contribution of the $n = 1$ trajectory to the TCS is also evident, corresponding to an f orbital electron attachment to form the negative ion, $Rb^-$ which subsequently decays.

To investigate the Wigner threshold law in the e⁻-Rb scattering, we first multiply the cross sections of Figure 6a by $k^2$ and plot the resultant data versus $E$. The results (dashed curves) are presented in Figure 6b together with those of Felfli et al.[29] (solid curves); they clearly exhibit a d-wave Wigner threshold law. To our knowledge, this is the first time that a d-wave has been found to determine the Wigner threshold law, the Ramsauer−Townsend minimum, and a d-resonance centered at 0.435 eV, all identifiable through even the TCS. These interesting results call for experimental and other theoretical confirmation.

The 3-D differential cross section is plotted as functions of both angle and energy in Figure 7, demonstrating that it does, indeed, exhibit the resonance structure manifested by the cross sections in Figure 6a near threshold. A careful examination of the DCS near threshold does lead to the determination of the critical minima.[18] Figure 8 (dashed curve) demonstrates clearly the position of the DCS's critical minimum, found at $E = 0.054$ eV when $\theta = 180°$. Also included in the figure are the data of Felfli et al.[29] with $b = 0.040$ (continuous curve). For all the angles shown in Figure 8, namely, 0°, 90°, and 180°, the resonance corresponding to Re $L = 4$ is clearly visible in the DCSs at $E = 1.73$ eV, being most significant at $\theta = 180°$. These results are attractive to both experimental and theoretical investigations, particularly very near threshold.

**e⁻−Cs.** The details of the analysis of the e⁻−Cs scattering are similar to those for the e⁻- K and e⁻−Rb scattering. Therefore, only significant manifestations will be pointed out. As in the case of e⁻−Rb, there are eight Regge trajectories originating from the ground state of $U(r)$ potential, as shown in Figure 9. It is noted that for e⁻−Cs scattering, Thumm and

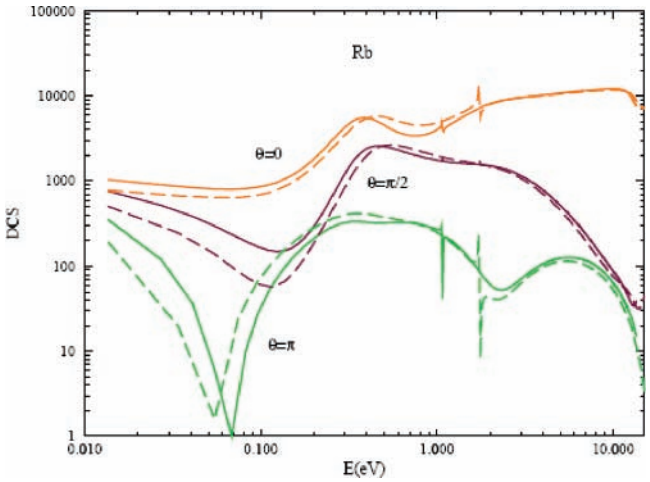


**Figure 8.** Differential cross sections for elastic e⁻−Rb scattering versus $E$(eV) at $\theta = 0°$, 90°, and 180° showing the DCS's critical minimum.

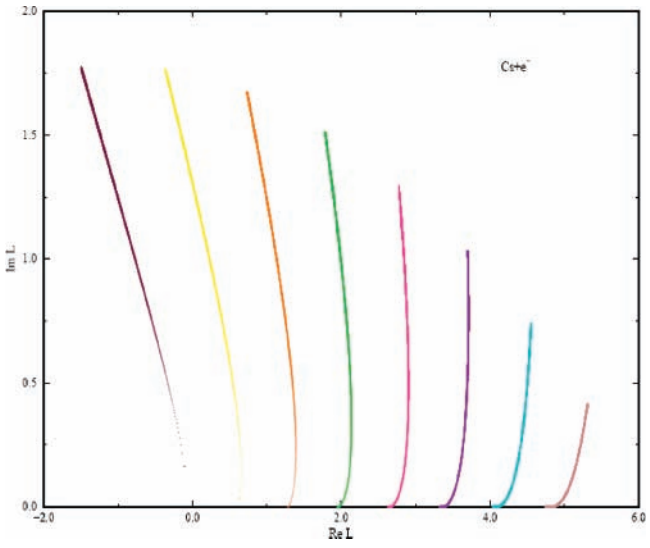


**Figure 9.** Regge trajectories, Im $L(E)$ versus Re $L(E)$ for $Cs^-$.

Norcross[30] demonstrated that the elastic TCS dominated the inelastic cross section in the energy range $0 \leq E \leq 2.8$ eV and found the R−T minimum at 0.046 eV. Previously, some data were presented[23] for the e⁻−Cs collision, focusing specifically

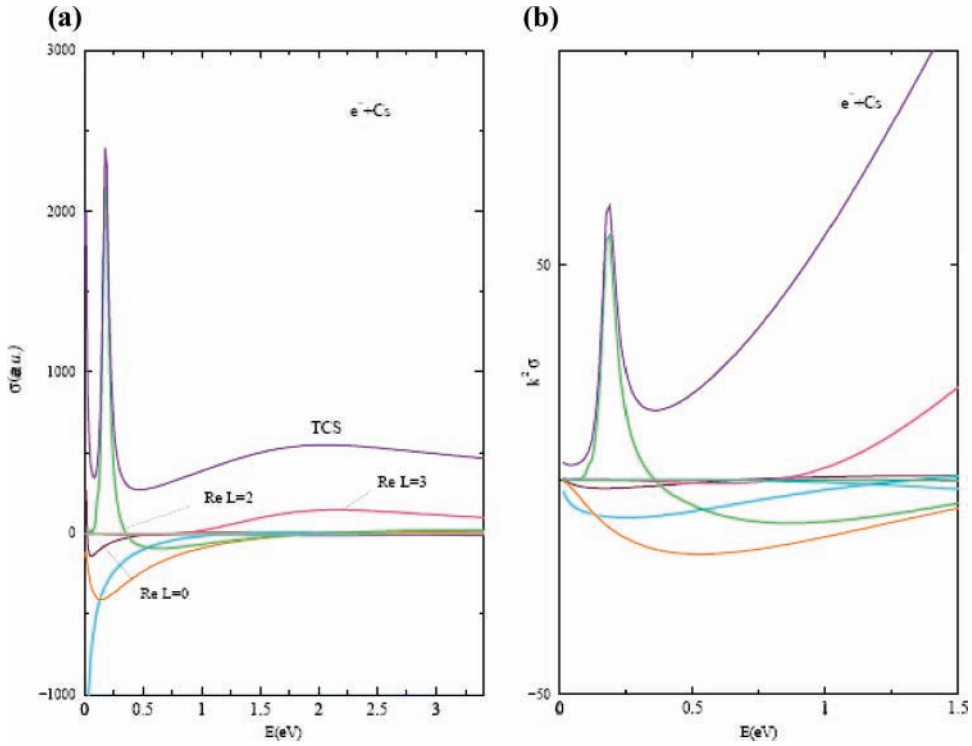


**Figure 10.** (a) The total and partial elastic cross sections, in atomic units, for $e^-$−Cs versus $E$(eV), showing the Mulholland contributions. (b) The total and partial elastic cross sections, in atomic units, for $e^-$−Cs multiplied by $k^2$ (a.u.) versus $E$(eV), showing the Mulholland contributions.

on the R−T minimum, found at $E = 0.048$ eV, in agreement with the above value.

Only the important Regge trajectories responsible for the structure in the TCS of Figure 10a will be considered here. The $n = 4$ (Re $L = 2$), $n = 3$ (Re $L = 3$), and $n = 7$ (Re $L = 0$) trajectories pass near integer values and are therefore likely to contribute to the peaks in the TCS. Indeed, the resonances at threshold (Re $L = 0$), at 0.17 eV (Re $L = 2$), and at ∼2.04 eV (Re $L = 3$) are accounted for by the $n = 7$, 4, and 3 trajectories, respectively. As seen from Figure 10a, the s-wave and d-wave partial cross sections define the R−T minimum, also visible in the TCS. The Regge partial cross section corresponding to Re $L = 3$ explains the broad resonance in the TCS centered at ∼2.04 eV. Figure 10a demonstrates that the electron attaches itself preferentially to the Re $L = 2$ orbital in forming the resonance centered around 0.204 eV. Note the combination of the d-wave and the s-wave to define the R−T minimum and that the near-threshold behavior is dominated by a d-wave, but which ultimately closes with a small s-wave component.

To extract the Wigner threshold law as before, we multiplied the cross sections by $k^2$ and plotted the results as depicted in Figure 10b. Clearly, a d-wave dominates the Wigner threshold behavior. Interestingly, the second minimum in the TCS is defined by the Regge partial cross section corresponding to Re $L = 2$ crossing zero, whereas the Regge f-wave partial cross section builds up to eventually maximize at about $E = 2.04$ eV.

The 3-D differential cross section in both angle and energy, emphasizing the phase that yields the highly peaked values and rich structure, is presented in Figure 11. Clearly, near threshold, the DCS exhibits a structure that is peaked in the forward direction. Figure 12 shows the critical minima of the DCSs at $\theta = 0°$, 90°, and 180°. The values of $E = 0.16$ eV and $\theta = 180°$ define the critical minimum for the $e^-$−Cs scattering.

For each of the three alkali metal atoms considered above, the near threshold electron elastic scattering resonance structure, Ramsauer−Townsend minima, Regge partial cross sections, TCSs, DCSs, and DCS critical minima are completely different from one another. Each atom has its own Wigner threshold characteristic behavior, being most interesting and complicated for $e^-$-K scattering. For this case, the Wigner threshold behavior can be extracted from the TCS only through scrutiny of Regge partial cross sections (compare Figure 2a and b).

## IV. Summary and Conclusion

We have demonstrated that Regge trajectories calculated within the CAM representation of scattering can be used to investigate and analyze the near-threshold formation of negative ions as Regge resonances in $e^-$−K, $e^-$−Rb, and $e^-$−Cs scattering. We found that the near-threshold electron collisions in these systems are characterized by the Wigner threshold law, Ramsauer−Townsend minima, and resonances, all discernible through Regge partial cross sections scrutiny. Additionally, the interesting results have been discovered for the $e^-$−Rb scattering: a d-wave Wigner threshold law, a d-wave R−T minimum, and a d-wave resonance centered around 0.435 eV, all identifiable through even the TCS, and that near-threshold electron attachment is preferentially to a d orbital to form the temporary $Rb^-$ ion. The sharp resonance at 1.727 eV is also identifiable through the DCS and is prominent at $\theta = 180°$, thus permitting experimental verification. It is noted that the measurement at $\theta = 180°$ gives the possibility to peer into the near-threshold energy region.

In $e^-$−Cs scattering, the near-threshold electron attachment is predominantly to a d orbital, and the combined s- and d-waves define the R−T minimum. In the $e^-$−K scattering, the near-threshold dynamic interplay among the s-, p-, and f-wave Regge partial cross sections modifies the position, magnitude, and shape of the R−T minimum. Also hidden within the innocent-looking TCS is the well-defined substructure extractable only through scrutiny of Regge partial cross sections (see Figure 2a). Through the Regge trajectory analysis, the dominant orbital to which the

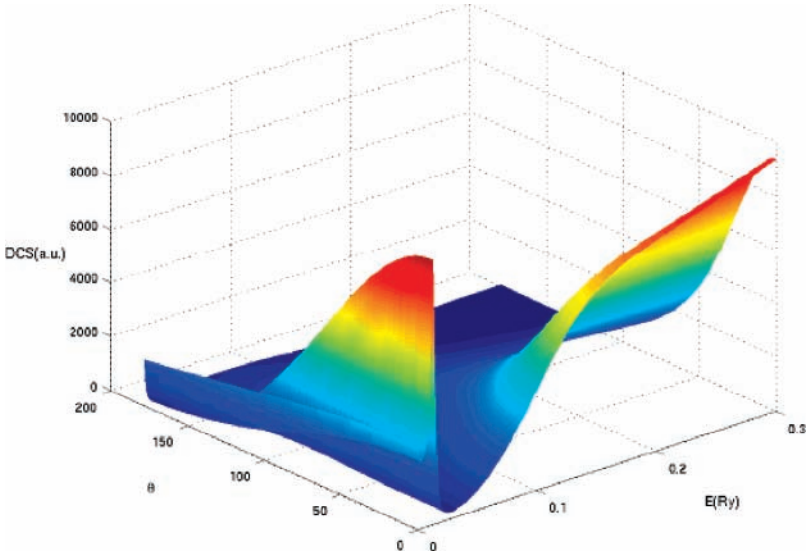


**Figure 11.** Three−D differential cross sections for elastic e$^-$−Cs scattering versus $E$(Ry) and $\theta$ (degrees).

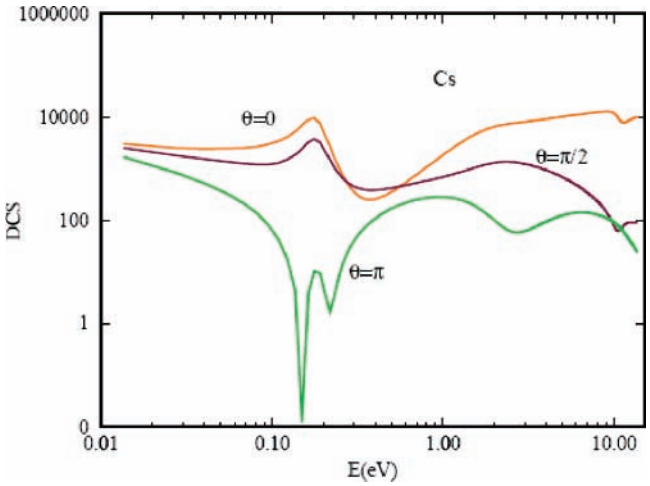


**Figure 12.** Differential cross sections for elastic e$^-$−Cs scattering versus $E$(eV) at $\theta = 0°$, 90°, and 180° showing the DCS's critical minimum.

electron preferentially attaches itself to form the temporary negative ion can be determined readily, including the possibility of determining the electron affinities of tenuously bound negative ions.[31]

The near-threshold cross section behaviors for e$^-$-K and e$^-$-Rb are significantly different from each other and revealing. One cannot say a priori by merely looking at the results for K$^-$ to what orbital the extra electron in Rb$^-$ will attach. A careful examination of the positions of the $n$d and ($n$ + 2)s excited orbitals in the neutral atoms provides the necessary clarification. In K, the 5s orbital is below the 3d orbital in energy but very close to it: 21 026.8 cm$^{-1}$ and 21 536.75 cm$^{-1}$, respectively. However, in Rb, the 4d is below the 6s orbital (also relatively close to it), with energies 19 355.45 and 20 133.6 cm$^{-1}$ respectively, whereas in Cs, the 5d is also below the 7s, with energies of 14 499.49 and 18 535.51 cm$^{-1}$, respectively. Clearly, the switching between the $n$d and the ($n$ + 2)s orbitals occurs between K and Rb. Consequently, there is a switching of the orbitals in moving from K$^-$ to Rb $^-$; this clarifies the entirely different near-threshold behavior for the two negative ions. The interesting consequence of this switching of the $n$d and ($n$ + 2)s orbitals as one moves from K through Rb to Cs is also discussed elsewhere in the context of the electron affinities for Ca$^-$ and Sr $^-$ and the attendant orbitals to which the extra electron preferentially attaches itself in forming the relevant negative Sr$^-$ ion.[31]

We conclude by noting that a short-lived resonance whose angular life is on the order of one full rotation may produce an oscillatory behavior in the energy dependence of the integral elastic cross sections, and this has recently been demonstrated using the F + $H_2$ reaction.[25] Finally, the present near-threshold data are expected to alleviate the lack of threshold scattering parameters, such as elastic cross sections and the attendant understanding of the collision dynamics, which has severely curtailed the utilization of particularly K in Bose−Einstein condensation. Finally, the paper has benefited immensely from the recent careful analysis of the low-energy electron scattering from gaseous $CS_2$[32] and the delineated resonance structures very close to threshold present experimental challenges.

**Acknowledgment.** This work was supported by the U.S. Department of Energy, Division of Chemical Sciences, Office of Basic Energy Sciences, Office of Energy Research. D.S. acknowledges financial support through an EPSRC (UK) grant.

## References and Notes

(1) Field, D.; Jones, N.; Ziesel J.-P. *Europhys. News* **2002**, *33*, 1.
(2) Kasdan, A.; Lineberger W. C. *Phys. Rev. A: At., Mol., Opt. Phys.* **1974**, *10*, 1658.
(3) Egorov, D. M. *Buffer-Gas Cooling of Diatomic Molecules*. Ph.D. Thesis, Harvard University, 2004.
(4) Bodo, E.; Gianturco, F. A.; Balakrishnan, N.; Dalgarno, A. *J. Phys. B* **2004**, *37*, 3641.
(5) Krems, R. V.; Dalgarno, A.; Balakrishnan, N.; Groenenboom, G. C. *Phys. Rev. A: At., Mol., Opt. Phys.* **2003**, *67*, 060703 (R).
(6) Kerman, A. J.; Sage, J. M.; Sainis, S.; Bergeman, T.; DeMille, D. *Phys. Rev. Lett.* **2004**, *92*, 033004.
(7) Aubin, S.; Myrskog, S.; Extavour, M. H. T.; LeBlanc, L. J.; McKay, D.; Stummer, A.; Thywissen, J. H. *Nat. Phys.* **2006**, *2*, 384.
(8) Zivanov, S.; Ibanescu, B. C.; Paech, M.; Poffet, M.; Baettig, P.; Sergenton, A.-C.; Grimme, S.; Allan, M. *J. Phys., B* **2007**, *40*, 101.
(9) Wigner, E. P. *Phys. Rev.* **1948**, *73*, 1002.
(10) Frautschi, S. C. *Regge Poles and S-Matrix Theory*; W. A. Benjamin: New York, 1963; Chapter X.
(11) de Alfaro, V.; Regge, T. *Potential Scattering*; North-Holland: Amsterdam, 1965).
(12) Connor, J. N. L. *J. Chem. Soc. Faraday Trans.* **1990**, *86*, 1627.
(13) Lengyel, V. I.; Navrotsky, V. T.; Sabad, E. P. *Resonance Phenomena in Electron-Atom Collisions*; Springer-Verlag: Berlin, 1992; Chapter 7.

(14) Chen, Z.; Msezane, A. Z. *J. Phys. B* **2000**, *33*, 5397.
(15) Bettega, M. H. F.; Winstead, C.; McKoy, V. *Phys. Rev. A: At., Mol., Opt. Phys.* **2006**, *74*, 022711.
(16) Andersen, T.; Haugen, H. K.; Hotop, H. *J. Phys. Chem. Ref. Data* **1999**, *28*, 1511.
(17) Bilodeau, R. C.; Bozek, J. D.; Gibson, N. D.; Walter, C. W.; Ackerman, G. D.; Dumitriu, I.; Berrah, N. *Phys. Rev. Lett.* **2005**, *95*, 083001.
(18) Milosavljevic, A. R.; Kelemen, V. I.; Filipovic, D. M.; Kazakov, S. M.; Pejcev, V.; Sevic, D.; Marinkovic, B. P. *J. Phys. B* **2005**, *38*, 2195 and references therein.
(19) Macek, J. H.; Krstić, P. S.; Ovchinnikov, S. Yu. *Phys. Rev. Lett.* **2004**, *93*, 183203.
(20) Sokolovski, D.; Felfli, Z.; Ovchinnikov, S. Yu.; Macek, J. H.; Msezane, A. Z. *Phys. Rev. A: At., Mol., Opt. Phys.* **2007**, *76*, 026707.
(21) Sokolovski, D.; Aquilanti, V.; Cavalli, S.; de Fazio, D. *J. Chem. Phys.* **2007**, *126*, 12101.
(22) Mulholland, H. P. *Proc. Camb. Phil. Soc. (London)* **1928**, *24*, 280.
(23) Felfli, Z.; Msezane, A. Z.; Sokolovski, D. *J. Phys. B* **2006**, *39*, L353.
(24) Bahrim, C.; Thumm, U.; Fabrikant, I. I. *Phys Rev. A: At., Mol., Opt. Phys.* **2001**, *63*, 042710.
(25) Sokolovski, D.; Felfli, Z.; Msezane, A. Z. *Bull. Am. Phys. Soc.* **2007**, *52*, 96.
(26) Belov, S.; Avdonina, N. B.; Felfli, Z.; Marletta, M.; Msezane, A. Z.; Naboko, S. N. *J. Phys. A* **2004**, *37*, 6943.
(27) Burke, P. G.; Tate, C. *Comp. Phys. Commun*. **1969**, *1*, 97.
(28) Savukov, I. M. *Phys. Rev. Lett.* **2006**, *96*, 073202.
(29) Felfli, Z.; Msezane, A. Z.; Sokolovski, D. *Eur. J. Phys.* **2007**, Submitted.
(30) Thumm, U.; Norcross, D. W. *Phys. Rev. A: At., Mol., Opt. Phys.* **1992**, *45*, 6349.
(31) Felfli, Z.; Msezane, A. Z.; Sokolovski, D. *J. Phys. B* **2007**, submitted.
(32) Gianturco, F. A.; Stoecklin, T. *Eur. Phys. J. D* **2006**, *42*, 85.